A simulation study of linker vacancy distribution and its effect on UiO-66 stability

Microporous and Mesoporous Materials 366 (2024) 112922

Contents lists available at ScienceDirect

Microporous and Mesoporous Materials

journal homepage: www.elsevier.com/locate/micromeso

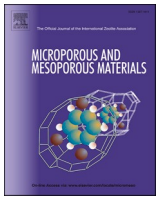

A simulation study of linker vacancy distribution and its effect on UiO-66 stability

Esteban Acuna-Yeomans [a,d], J.J. Gutiérrez-Sevillano [b,**], David Dubbeldam [c], Sofia Calero [a,d,*]

[a] Materials Simulation and Modelling, Department of Applied Physics and Science Education, Eindhoven University of Technology, 5600, MB Eindhoven, the Netherlands
[b] Department of Physical, Chemical and Natural Systems, Universidad Pablo de Olavide, Ctra. Utrera Km. 1, 41013, Seville, Spain
[c] Van 't Hoff Institute for Molecular Sciences, University of Amsterdam, Science Park 904, 1098XH Amsterdam, the Netherlands
[d] Eindhoven Institute for Renewable Energy Systems (EIRES), Eindhoven University of Technology, P.O. Box 513, 5600, MB Eindhoven, the Netherlands

ARTICLE INFO

Keywords:
UiO-66
Defect engineering
MOFs
Mechanical stability
UiO-66 amorphization
Elastic moduli anisotropies

ABSTRACT

In this work, we computationally investigate the impact of the distribution of linker vacancies on the relative stability of defected UiO-66 structures. Analysis of a significant number of defected structures reveals that higher defect numbers correlate with lower stability, but variations in missing linker distribution and orientation contribute to widely differing amorphization pressures. Our results suggest that structures with more evenly distributed vacancies exhibit a positive linear relationship between amorphization pressure and bulk modulus. Furthermore, we found structures with a disproportionate number of missing linkers with the same orientation and structures where a large volume of the framework remains pristine, display outlier behavior in this respect. Evaluation of anisotropic elastic moduli uncovers directional instability in structures with a high number of vacancies with the same orientation. These findings have important implications for designing and optimizing UiO-66-based materials, aiding in defect configuration selection for specific applications.

1. Introduction

Metal-organic frameworks (MOFs) have continued to receive attention from the scientific community at large ever since the first ones were synthetized more than twenty years ago [1–3]. These materials consist of metal clusters coordinated with organic ligands forming ordered crystal lattices [4–6]. Their porous structure and possibility of ligand functionalization make them an appealing alternative in applications such as catalysis [7–10], drug delivery [11] and gas storage and separation [12–15].

In the last decade the archetypal MOF, UiO-66 [16], has received considerable attention within the field due to its high hydrothermal [17–19] and mechanical stability [18,20], even under high-pressure conditions. The structure of UiO-66 is characterized by zirconium-based Zr_6 O_4 $(OH)_4$ clusters bridged to one another via 1, 4-benzenedicarboxylic acid (BDC) ligands. In the pristine (defect-free) material each inorganic cluster is 12-fold coordinated, that is, each cluster is connected to the others by 12 BDC linkers. The high structural stability of UiO-66 and its extended sibling materials (UiO-67 and UiO-68) has been attributed to the high coordination number of its inorganic clusters (12) compared other prototypical MOFs such as ZIF-8 (4) and MOF-5 (6) [21].

The vast majority of synthesis procedures for UiO-66 result in a defected structure with missing linkers [7,22,23]. Thermogravimetric analysis (TGA) measurements suggest that for the less defected UiO-66 samples the coordination number of each zirconium cluster is 11, indicating one missing linker on average [17,24]. This observation has been further verified via NMR7, X-ray and neutron diffraction [25,26] and IR/Raman spectroscopy experiments [24]. The presence of linker defects increases the porosity and available surface area of the material, which modifies the adsorption behavior [26–29], catalytic properties [7, 30], proton conductivity [31,32] and thermal stability [33] of it. The tradeoff between enhancement in adsorption and the effect on stability when defects are introduced is an ongoing research topic, which often requires the use of computational techniques in order to analyze the relationships between specific properties and the structure of the material, on a molecular scale.

In the past decade, computational simulations have been used to

* Corresponding author. Materials Simulation and Modelling, Department of Applied Physics and Science Education, Eindhoven University of Technology, 5600, MB Eindhoven, the Netherlands.
** Corresponding author.
E-mail addresses: jjgutierrez@upo.es (J.J. Gutiérrez-Sevillano), s.calero@tue.nl (S. Calero).

https://doi.org/10.1016/j.micromeso.2023.112922
Received 25 July 2023; Received in revised form 24 November 2023; Accepted 26 November 2023
Available online 29 November 2023

study the adsorption properties of both pristine and defected UiO-66, often with the focus on water and CO2 adsorption [27,29,34–38]. These have provided substantial insight for industrial applications such as water harvesting and gas separation. The simulations involved in most of these works often model UiO-66 as a rigid structure, where the framework only interacts with the guest molecules via non-bonded potentials.

The computational study of structural and mechanical properties of UiO-66, specially at high pressures, requires for the framework to be modelled as flexible. Several classical force fields (FFs) have been proposed in order to gain atomistic understanding of the underlying mechanisms that control the flexible behavior of the system. In an early work, Boyd et al. [39] modelled pristine UiO-66 using both the Universal Force Field (UFF) [40] and its extension for MOFs, UFF4MOF [41], without taking into account electrostatic contributions from point charges to the potential energy. They found that they could reproduce the structural properties of the defect-free structure at ambient conditions and provide a reasonable approximation of its bulk modulus under the same conditions. Upon testing the system using three different sets of point charges (CBAC, REPEAT, Qeq), they noted that it results in unpredictable behavior with respect to the bulk modulus. In 2014, Bristow et al. [42] proposed an ab-initio derived force field for a slew of prototypical MOFs, including UiO-66, which proved capable of accurately estimating the structural parameters and the volumetric heat capacity of the material, however, it severely underestimates the bulk modulus. Said FF has seldom been used in computational studies since it was proposed, and hence validation and comparison with experimental measurements is lacking.

The only reported classical flexible approach that is able to provide interaction parameters for defected UiO-66 structures and has been extensively validated is the one proposed by Rogge et al., in 2016 [43], which consists of constructing ab-initio derived force fields for each particular structure via the QuickFF procedure [44]. They found that for the pristine structure, applying external pressure to the system induces short range disorder and loss of crystallinity at a pressure of 1.83 GPa. Analysis of the elastic constants at high pressure shows a breakage of the second Born stability criterium, indicating that high-pressure amorphization in the framework is caused by compression.

In their work, they constructed 8 different force fields for 8 distinct defected structures with one or two defects per UiO-66 unit cell. They estimated the pressure-versus-volume equations of state for each structure, and determined that defects have a minor effect on the equilibrium volume but introduce a substantial and gradual decrease in the amorphization pressure and the bulk modulus. They found that the most profound effect on the stability of the defected system is obtained when the linker vacancies share the same orientation but lie in neighboring lattice planes.

To better understand the full impact of defects on the stability of UiO-66, it is essential to mechanically characterize a large number of defected structures. Mainly, the necessity of compensating the charge of the missing linkers in order to maintain a system with zero net charge effectively means that for every structure with a different number and distribution of defects, a distinct set of charges and thus a distinct force field, must be used. This represents a limiting factor for the computational screening of large number of defected structures.

In this work we model all defected UiO-66 structures using the same force field (UFF) without taking into account electrostatic interactions, to zero-in on the effect that the number, distribution and orientation of missing linkers has on the mechanical properties of the system. In order to validate our proposed methodology, we reproduced the defected structures studied by Rogge et al. [43], estimated both the amorphization pressure and bulk modulus of each one and compared them with their results. We found that although the quantitative values for them differ considerably (by a factor of ~2.7 for the pristine material), the trends followed by the two sets of estimations are highly correlated, indicating that although our methodology is not able to provide realistic estimations of the mechanical and structural properties, it is helpful for analyzing the stability of different defected structures relative to each other.

During the course of this project we generated over 100 UiO-66 structures ranging from 1% defected to 18% defected, with varied missing linker spatial concentration, orientation and order. The amorphization pressure and elastic stress tensor for all structures were computed using molecular dynamics (MD) simulations and subsequently processed, analyzed and contrasted with each other. Our results are able to provide greater insight on how linker distribution is related to the mechanical stability of material.

2. Methodology

In this study, we aim to investigate the stability of defected UiO-66. To this end, we examined two broad categories of defective structures (see Fig. 1). The first type involved structures with a regular arrangement of linker vacancies, which were generated by replicating a defected conventional unit cell to create a 2 × 2 × 2 supercell. The second type consisted of structures with irregular linker vacancies created directly at the supercell level. To introduce these disordered vacancies, we employed various methods, such as random removal or quasi-random removal of linkers in the pristine structure. The latter approach involved selectively removing linkers in accordance with specific criteria, such as removal from specific sub-volumes of the supercell or based on particular linker orientations.

To identify factors that might contribute to structural stability, we characterized each defected structure according to five metrics: (1) the mean distance between linker vacancies, where the position of each missing linker was taken to be the geometric center of the benzene ring, (2) the mean distance from the linker vacancies to the geometric center of the 2 × 2 × 2 supercell, (3) the radial distribution of linker vacancies with respect to the center of the supercell, (4) the amounts of missing linkers with a particular orientation, and (5) the amount of inorganic clusters with a particular coordination contained in the structure. Most of the metrics are included in the supporting information file, only the most useful at distinguishing mechanical behavior between structures with the same number of linker vacancies are included and referred to in the main text.

In this study we decided to model the defected UiO-66 structures using the Universal Force Field [40]. For this, we chose to exclude electrostatic contributions from the potential energy. It eliminates the need to compensate for the charge of removed organic linkers with approaches such as the redistribution of charges in the remaining structure [38] or the inclusion of ions to cap defected cluster sites [28], both of which would significantly restrict the number of defected structures that could potentially be considered in this study. Importantly, in our experience, the inclusion of ions in the pore volume reduces the space available for the framework to ‘collapse into’. It affects the volume change of the system during the simulations, inhibiting the methodology used in this study to determine if a collapse occurred. Additionally, although the computational cost of including short-range electrostatics would be relatively low in a per-simulation basis, the sum total for all runs using our methodology would be significant. The UFF energy equation is defined as:

$$U = U_{\text{bonded}} + U_{\text{non-bonded}} \tag{1}$$

where

$$U_{\text{bonded}} = U_{\text{bonds}} + U_{\text{angles}} + U'_{\text{angles}} + U_{\text{dihedrals}} + U_{\text{impropers}}$$

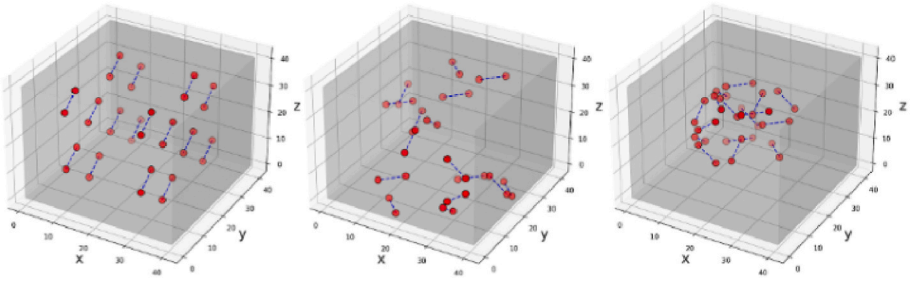

Fig. 1. Pictorial representation of 3 different defected UiO-66 structures with an average cluster coordination of 11 at the supercell level. The linker vacancies are represented by dashed blue lines, the red end points represent the missing connection with inorganic clusters and the grey volume represents the non-defected part of the framework. Transparency of the red and blue colors is used to aid depth perception, fuller colors mean that the vacancy is located closer to the point of view of the observer, more transparent colors mean that the vacancy is located further away. The first image pictures the framework containing 16 vacancies with a regular arrangement while the second and third images are examples of structures with an irregular arrangement of vacancies, where the 16 organic linkers were removed randomly and quasi-randomly, respectively.

$$
\begin{aligned}
&= \sum_{\text{bonds}} \frac{1}{2} K_r (r - r_0)^2 + \sum_{\text{angles}} \frac{K_\theta}{n^2} [1 - \cos(n\theta)] + \sum_{\text{angles}} K_\theta [C_0 + C_1 \cos(\theta) \\
&+ C_2 \cos(2\theta)] + \sum_{\text{dihedrals}} \frac{K_\varphi}{2} [1 - \cos(m\varphi_0)\cos(m\varphi)] \\
&+ \sum_{\text{improper}} K_\xi [C_0 + C_1 \cos(\xi) + C_2 \cos(2\xi)]
\end{aligned} \tag{2}
$$

$$
U_{\text{non-bonded}} = \sum_{\text{pairs}} 4\epsilon_{ij} \left[\left(\frac{\sigma_{ij}}{r_{ij}} \right)^{12} - \left(\frac{\sigma_{ij}}{r_{ij}} \right)^{6} \right] \tag{3}
$$

In the bonded term, r is the bond distance while θ. φ, and ξ are the bend, dihedral and improper dihedral angles, respectively. The non-bonded part consists of the van der Waals interaction between a pair of atoms i and j separated by a distance r_{ij} where σ_{ij} and ϵ_{ij} refer to the equilibrium distance and well depth of the potential, respectively. The first angle term in the bonded potential applies to atoms in linear, trigonal-planar, square-planar, or octahedral arrangement and the second angle term can be used for the general non-linear case. In the specific case of UiO-66, the second term is used to model the angle bending interactions inside the inorganic cluster of the types $O-Zr-O$, $H-O-Zr$ and $Zr-O-Zr$. The specific force field parameter values, their associated atom types and the definition of the angle bending and improper torsion coefficients, as used in this work, are described in the Supporting Information file.

In this study, we employ two complementary approaches to evaluate the stability of defective structures. The first approach, proposed by the Coudert group [45], involves assessing the anisotropy of the mechanical moduli of the structure. The uniaxial stiffness of the material in a given direction $\boldsymbol{u}$ is determined by Young's modulus $E(\boldsymbol{u})$, while the directional deformation caused by isostatic compression is measured by the linear compressibility modulus $\beta(\boldsymbol{u})$. The directional dependence of the moduli can be obtained from the inverse of the fourth-order elastic stiffness tensor $\mathbf{C}$ (also called the compliance tensor), by applying to it a rotation mapping the x axis onto the direction of the unit vector $\boldsymbol{u}$, and are calculated (Einstein's notation used) as [45,46]:

$$
E(\boldsymbol{u}) = \frac{1}{u_p u_q u_r u_s \left[\mathbf{C}^{-1}\right]_{pqrs}}, \beta(\boldsymbol{u}) = u_p u_q \left[\mathbf{C}^{-1}\right]_{pqrr} \tag{4}
$$

Where the u_x terms are the components of the rotation matrix. The anisotropy of each property is determined by calculating the ratio between its maximum and minimum values, which can range from 1 to infinity. This property reflects the flexibility of the material, where softer crystals exhibit large anisotropy factors, rigid MOFs are characterized by considerably lower values, close to unity [47].

The elastic stiffness tensor $\mathbf{C}$ at a particular temperature can be estimated via molecular dynamics simulations via the stress-fluctuation method. In the canonical ensemble, the equations for the stress tensor $\boldsymbol{\sigma}$ and for the elastic stiffness tensor reduce to Refs. [48,49]:

$$
\sigma_{\alpha\beta} = \langle \sigma^B_{\alpha\beta} \rangle - \rho k_B T \delta_{\alpha\beta} \tag{5}
$$

$$
\mathscr{C}_{\alpha\beta\mu\nu} = \langle \mathscr{C}^B_{\alpha\beta\mu\nu} \rangle - \frac{V}{k_B T} \left[\langle \sigma^B_{\alpha\beta} \sigma^B_{\mu\nu} \rangle - \langle \sigma^B_{\alpha\beta} \sigma^B_{\mu\nu} \rangle \right] + \rho k_B T \left(\delta_{\alpha\mu}\delta_{\beta\nu} + \delta_{\alpha\nu}\delta_{\beta\nu} \right) \tag{6}
$$

Where $\sigma^B_{\alpha\beta}$ and $\mathscr{C}^B_{\alpha\beta\mu\nu}$ are the Born stress tensor and the Born matrix, respectively. They are the first and second derivatives of the potential energy U with respect to strain, given by

$$
\sigma^B_{\alpha\beta} = \frac{1}{V} \frac{\partial U}{\partial \varepsilon_{\alpha\beta}} \quad \mathscr{C}^B_{\alpha\beta\mu\nu} = \frac{1}{V} \frac{\partial^2 U}{\partial \varepsilon_{\alpha\beta} \partial \varepsilon_{\mu\nu}} \tag{7}
$$

In this work, we computed the anisotropic elastic constants tensor of all defected structures both at 0K and at finite temperatures, in order to quantify their mechanical stability at a given temperature and pressure. Calculations at finite temperatures were carried out by following the stress-fluctuation technique using the born/matrix compute [50] recently implemented in the LAMMPS [51] molecular simulation package, which allows for the computation of elastic constants for arbitrary complex potential interactions. The 0 K elastic constants were calculated using the cell deformation technique using the same simulation package.

The second approach consists of determining the pressure versus volume behavior of the structure via molecular dynamics simulations in the flexible NPT ensemble (N, P, $\boldsymbol{\sigma_\alpha} = \mathbf{0}$, T), where the number of particles N is fixed while the internal pressure P_i, internal deviatoric stress $\sigma_{\alpha,i}$ and the internal temperature T_i are controlled. The ensemble allows for the dynamic change of both the simulation cell volume V and shape $\mathbf{h_0}$ and can be systematically used to estimate the pressure at which the framework amorphization takes place (P_{am}).

For each defective structure we conducted looped flexible NPT simulations starting from a sufficiently high pressure. At the start of each loop, energy minimization of the system is conducted, and the final volume V_r is saved. The instantaneous volume V_i was monitored during the equilibration period of each simulation. Amorphization was determined to have occurred if at any point during equilibration, the value of V_i became lower than a predefined volume threshold V_t, taken to be proportional to V_r. In the scenario where amorphization was determined to have occurred, the subsequent simulation within the loop would start with a pressure value that ΔP lower than the previous one. Conversely, if it was established that amorphization had not transpired, the pressure value of the following simulation in the loop would be increased by ΔP. The final characteristic P_{am} value for the particular structure would be determined to be the final pressure value at which the structure does not collapse plus ΔP. This approach has been widely used previously to study the stability of ZIFs and MOFs, although it has been noted that the fluctuations in instantaneous pressure inherent in MD simulations may

induce phase transitions at artificially low pressures [47,52]. In order to partially mitigate said fluctuations we employed sufficiently large simulation cells.

2.1. Computational details

The defected structures were generated using an in-house program which takes the force field parameters and the pristine UiO-66 structure crystallographic information file as inputs and outputs a LAMMPS topology data file.

All pressure versus volume MD simulations reported in this work were carried out in the flexible NPT (N, P, $\boldsymbol{\sigma_\alpha} = \mathbf{0}$, T) ensemble using the LAMMPS simulation package [51]. The simulation timestep used for the Verlet integrator was 0.5 fs to ensure energy conservation. During these simulations the temperature was fixed at 300 K and controlled via a Nose-Hoover chain thermostat using a relaxation time of 50 fs. The pressure control was handled by a MTTK barostat with a relaxation time of 500 fs. The pressure was modified according to the discussed looping simulations scheme, ΔP was set at 0.005 GPa and the volume threshold V_t was set at 0.8 times the volume of the structure after energy relaxation.

For the computation of the elastic stiffness tensor, the cell parameters and atomic coordinates of each structure were first relaxed and, once a minimum was reached, the stress tensor and Born matrix were sampled in 200 ps long NVT simulations in LAMMPS, using the numerical derivative method [50] for the latter. The temperature was fixed at 300 K and controlled via a Nose-Hoover chain thermostat with a relaxation time of 100 fs. The running average of the Born matrix was sampled every timestep using the born/matrix compute [50]. For each structure, using the ELATE python module [53] with the obtained elastic constants as input, the minimal/maximal values of linear compressibility β and Young's modulus E were estimated, as well as their corresponding anisotropy values.

All simulations were performed in a supercell of the defected structure using UFF without electrostatic contributions. Periodic boundary conditions were applied in all three dimensions. As per UFF indications, for each framework atom, a "scaled 1–4" policy was taken into account; that is, non-bonded interactions (VdW) between couples of bonded atoms (1–2) or between atoms bonded to a common atom (1–3) were excluded, while the interaction between atoms separated by two others (1–4) were fully considered.

3. Results and discussion

To determine the viability of our proposed methodology, we constructed the 8 defected structures studied by Rogge et al. [43]: one of them (type0) corresponds to a system with one linker vacancy per unit cell and the rest (type1-7) to structures in which an different additional linker defect is introduced to the type0 parent. In order to compare our methodology with those reported by them we calculated the amorphization pressure (P_{am}) and bulk modulus (K_V) of each; using the flexible NPT simulation scheme and the stress fluctuation technique in the NVT ensemble, respectively. The results are provided in Table 1.

Table 1
Comparison of amorphization pressure (P_{am}) and Bulk modulus (K_V) predicted by our methodology and those reported by Rogge et al. [43], respectively. Simulations conducted at a temperature of 300 K. All values in GPa.

Defect type	This work		Rogge et al.	
	$\mathbf{P}_{am}$	KV	$\mathbf{P}_{am}$	KV
Pristine	2.91	59.5	1.83	22.2
type0	2.53	56.4	1.55	19.9
type1	2.2	50.39	1.29	17.4
type2	2.24	52.22	1.37	18.2
type3	2.41	52.51	1.51	18.7
type4	2.31	51.51	1.39	18.2
type5	2.09	50.65	1.17	15.5
type6	2.44	53.45	1.38	18.9
type7	2.22	48.97	1.35	17.2

The results obtained in this study exhibit significantly greater quantitative values compared to those reported by them. Nevertheless, upon closer examination, it becomes apparent that the relative variances in properties between the two sets of results seem to be comparable. To delve deeper into this observation, we conducted an analysis of the relative trends among each set of defective structures. The outcomes of this analysis can be visualized in Fig. 2.

Fig. 2A and C demonstrate that the available experimental measurements provide strong support for the accurate predictive capabilities of the Rogge force field. Our results are qualitatively similar but differ quantitatively. Despite this quantitative discrepancy, the trends observed between the values in both sets remain relatively consistent. In terms of qualitative analysis, the computed properties for the various structures indicate similar conclusions concerning the relative stability of the reference defected structures. Specifically, the type5 structure, where the removed linkers have equal orientation on two different planes, is the least stable; and type3 and type6 structures are the most stable of the structures with average cluster coordination of 11.

In order to measure the degree of similarity between the relative values of the properties in both sets, we performed a calculation of the correlation coefficient. Fig. 2C and D illustrate the obtained results, revealing correlation coefficient values that are close to unity. This indicates a strong positive correlation between the two sets of amorphization pressure and bulk modulus values.

The preceding findings indicate that while our proposed methodology may not possess the quantitative capabilities to rival other existing schemes in terms of providing realistic values for mechanical properties, it is nonetheless well-suited for investigating the relative stability among defected structures.

Based on this conclusion regarding the suitability of our methodology for studying relative stability, we proceeded to generate a significant number of defected structures by varying the number, distribution, and orientation of linker vacancies. As a basis for future comparison we created a reference set of 8 structures with increasing number of defects (ranging from 4 to 32), where linker vacancies were introduced in an orderly fashion starting from the pristine baseline at the supercell level. As can be seen in Fig. 3, the pressure at which the structure collapses decreases when more defects are introduced and the obtained values are able to accurately predict the amorphization pressure simulated pristine structure, via linear extrapolation. In order to determine the degree to which the vacancy introduction process impacts the reference amorphization values, we generated an alternative reference set in which the same vacancies are introduced randomly. As can be seen in figures S1 and S2, the difference for both individual P_{am} values and trend is minimal between the sets.

Fig. 4 depicts the amorphization pressure for all the generated defected structures. Notably, a high amount of variance in P_{am} values is observed for structures with the same number of defects but different missing linker distribution and orientation. Comparing the values obtained for N = 8, 16, 24 and 32 linker defects, structures with a regular arrangement of vacancies tend to present extreme amorphization values, corresponding to the least and most stable structures in terms of P_{am}, whereas structures with irregular vacancies, where missing linker positions and orientations were selected either randomly or quasi-randomly tend to fall in the middle.

Comparison of amorphization pressure values between sets of structures with different number of vacancies reveals numerous cases in which structures with a higher number of vacancies are less prone to collapse at higher pressures than structures with fewer defects. This suggests that the number of linker vacancies alone does not solely determine the stability of the structure. Factors such as the selection method, distribution, and orientation of the defects significantly contribute to the variance in amorphization pressure, particularly for

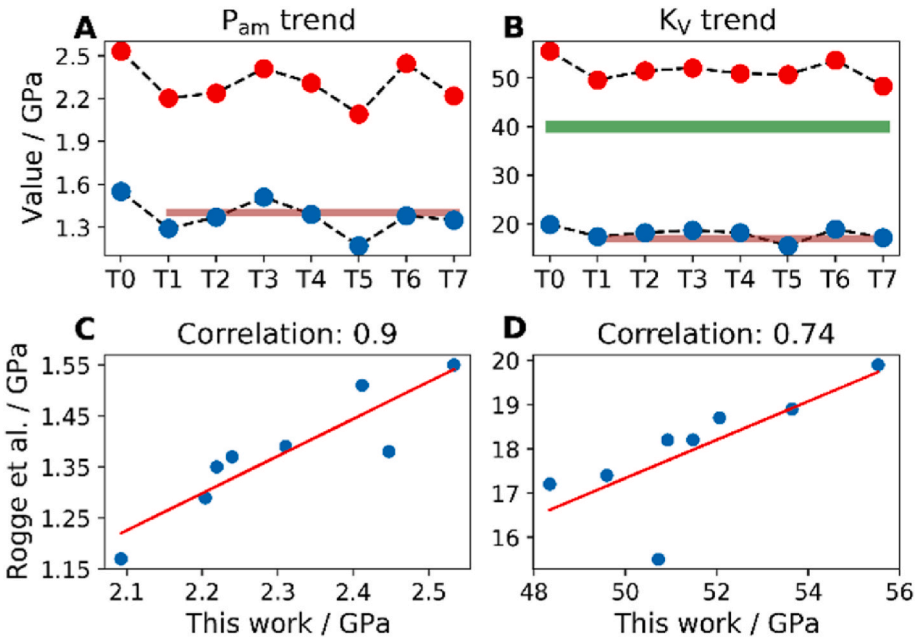

Fig. 2. Comparison of the amorphization pressure (A) and bulk modulus (B) trends for the 8 defected structures proposed by Rogge et al. [43] using both methodologies. The trends are also compared with the reported DFT values for the pristine structure [54] (green line) and the reported experimental measurement [20] for a structure of average metal coordination of 11 (brown line). The correlation coefficient for amorphization pressures and bulk modulus between the data sets is pictured in (C) and (D), respectively. For both cases a strong positive correlation is observed.

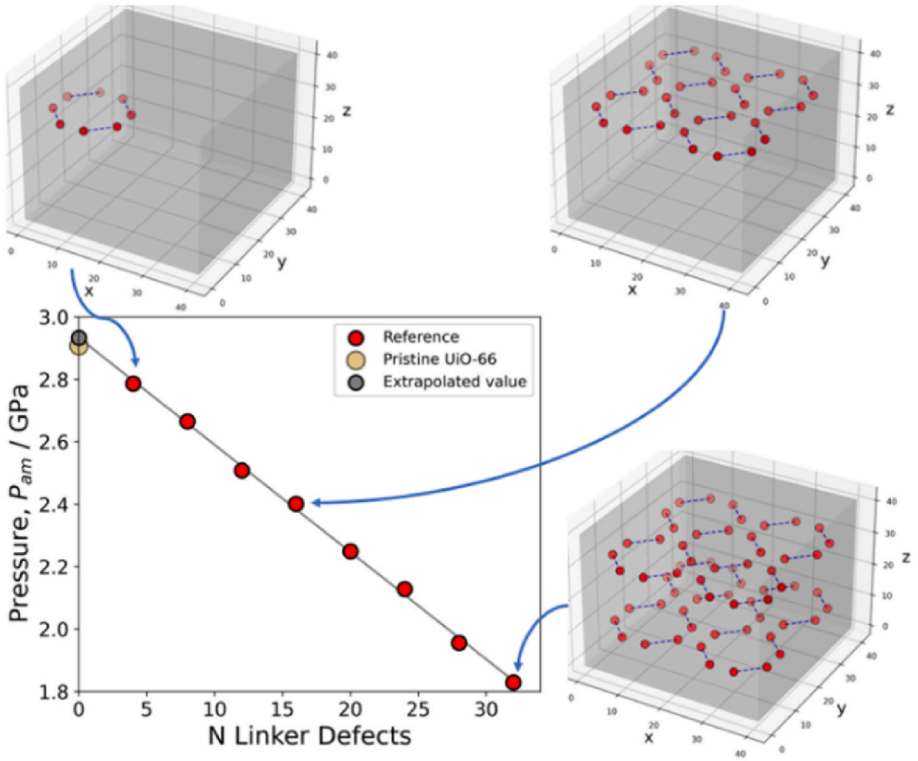

Fig. 3. Amorphization pressure with respect to the number of linker vacancies for the reference system, where linkers were taken out in order. Included are pictorial representations of the structures with 4, 16 and 32 linker vacancies. The line represents the linear extrapolation of the P_{am} values for the reference system. The extrapolated value using the reference system data is 2.934 GPa, which is close to the value obtained by simulating the pristine structure (2.908 GPa).

structures with a higher number of defects. As was the case for the reference system, in general, the amorphization pressure decreases as the number of defects in the structure increases.

Fig. 5 contrasts the results obtained for the reference system with the average amorphization pressure of each set of defected structures. Our results indicate that the amorphization pressure decreases linearly with increasing number of defects, where the linear trend obtained when taking into account all amorphization values is almost the same as the one obtained for the reference set.

As evidenced by the analysis of the structures proposed by Rogge

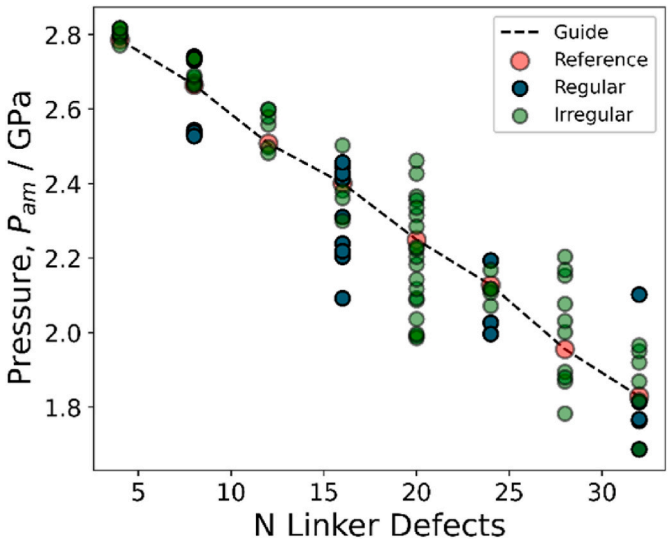

Fig. 4. Amorphization pressure with respect to the number of linker vacancies contained for all defected structures of study. Each data point corresponds to a defected structure with different vacancy spatial concentration, orientation and order. The dotted line is a visual guide that passes through the reference data. Data points are colored according to the structure generating procedure. High amount of variance in amorphization pressure values is obtained.

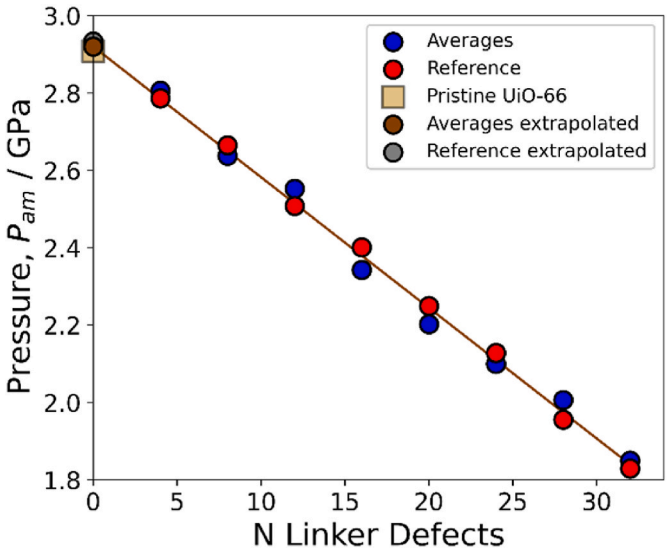

Fig. 5. Comparison between the reference system (red circles) and the average amorphization pressure value for each set of defected structures (blue circles). The line represents the linear extrapolation of the average values. The extrapolated Pam estimation for a structure with 0 linker defects is 2.92 GPa which is close to the amorphization pressure of the pristine structure obtained using MD (2.908 GPa).

et al. [43] amorphization pressure values do not provide a complete picture of the stability of the defected frameworks. To address this, we computed the 0 K elastic stress tensor for all structures and from them calculated the relevant elastic moduli. Comparison of amorphization pressure and bulk modulus values reveals that for structures with an irregular arrangement of defects selected randomly from the whole framework volume (which are most of the structures studied in this work) the amorphization pressure is related to the bulk modulus in a positively linear way. Furthermore, said structures tend to have a homogeneous distribution of missing linker orientations, meaning that they don't usually contain a disproportional number of missing linkers of one orientation type. Most of the structures generated quasi-randomly where defects were created in sub-volumes of the framework exhibit similar behavior. Fig. 6 shows the relationship between amorphization pressure and bulk modulus for a representative subset of the structures containing 20 linker vacancies.

In general, we observe that structures where the vacancies are more evenly distributed, both spatially and in orientation, follow the linear trend evidenced by the green data points in the figure. Structures where most of the missing linkers had the same orientation (blue data point) and structures with quasi-randomly distributed vacancies that leave a large part of the volume as pristine (red data point) tend to exhibit outlier behavior in this respect.

Further examination of the outlier structures reveals that cases in which the vacancies are distributed in a way that a large volume of the structure remains pristine (Fig. 7A) exhibit greater stability, evidenced by a large bulk modulus and amorphization pressure value. Analysis of elastic moduli anisotropies (Fig. 7B) is required in order to reveal the directional instability exhibited by structures containing a large number of vacancies with the same orientation. We find that in these cases, low amorphization pressure values correspond to high elastic moduli anisotropies.

4. Conclusions

In this work we aimed to investigate the influence of different distributions of linker vacancies on the relative stability of defected UiO-66 structures. We employed the same force field (UFF) for modeling all defected structures without considering electrostatic interactions. While our approach may not match the quantitative accuracy of other existing schemes in predicting structural and mechanical properties, it proved suitable for examining relative stability among defected structures.

Through our investigation, we analyzed a significant number of defected structures by manipulating the number, distribution, and orientation of linker vacancies. As expected, our initial analysis revealed that structures with a higher number of defects exhibit lower stability compared to those with fewer defects. Interestingly, we observed significant variation in amorphization pressure values for structures with the same number of defects but different missing linker distributions. This suggests that the stability of a structure is not solely determined by

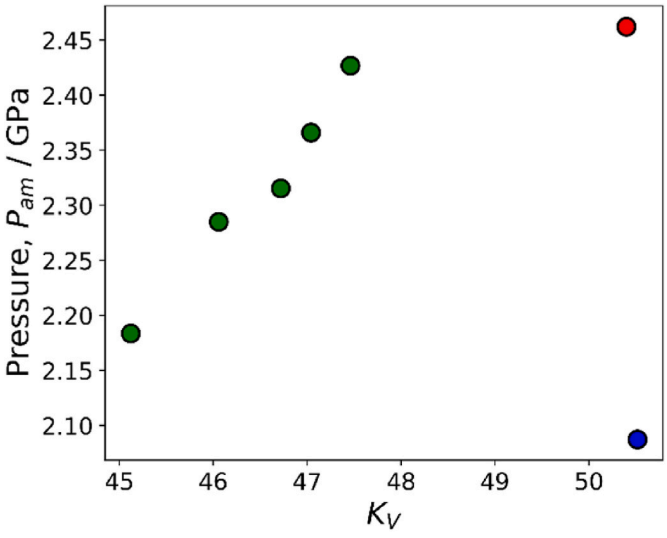

Fig. 6. Relationship between amorphization pressure and bulk modulus for a representative subset of the structures containing 20 linker vacancies. Most of the studied defected structures follow the trend represented by the green data points where a positive linear relationship between the amorphization pressure and bulk modulus is observed. Outlier structures with high bulk modulus and contrasting Pam represented with red and blue circles.

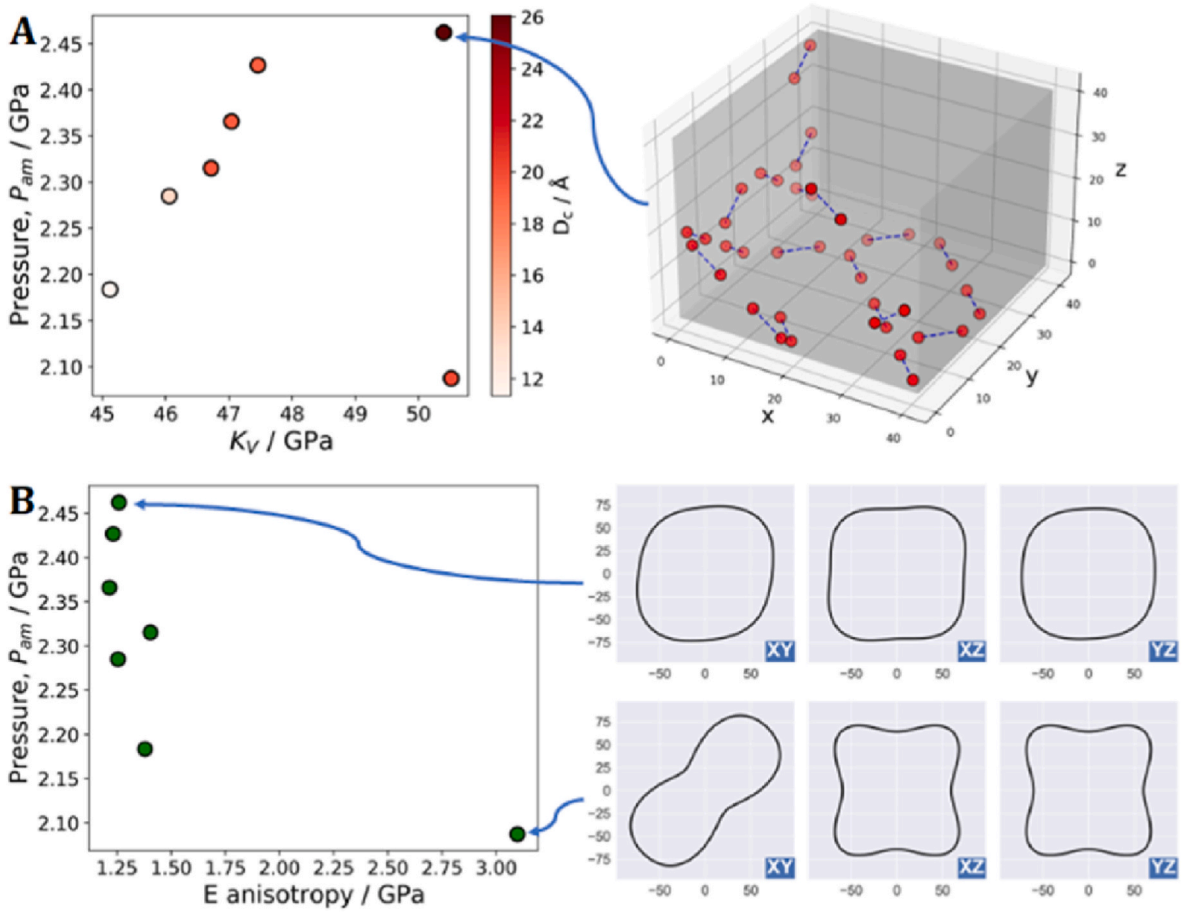

Fig. 7. Analysis of the representative outlier structures pictured in Fig. 6. In plot (A), every data point is color coded according to the mean distance between the linker vacancies and the center of the 2 × 2 × 2 simulation cell (in angstroms). Plot (B) shows the amorphization pressure with respect to the Young modulus' anisotropy for the same structures. The polar plots in the bottom, contrasting the Young modulus anisotropies for two of the representative structures were generated using the ELATE python module [53].

the number of linker vacancies, but also influenced by factors such as the selection method, distribution, and orientation of the defects.

Furthermore, when comparing amorphization pressure and elastic moduli values, we found that structures with more evenly distributed vacancies, both spatially and in orientation, exhibited a positive linear relationship between amorphization pressure and bulk modulus. In contrast, structures with imbalanced missing linkers of the same orientation or quasi-randomly distributed vacancies where a substantial portion of the volume remains pristine, exhibited outlier behavior in this regard.

To gain a comprehensive understanding of the behavior of outlier defected structures, it is crucial to analyze the anisotropies of elastic moduli, particularly for structures containing a significant number of vacancies with the same orientation. Our study revealed that in such cases, structures with low amorphization pressure values exhibited high elastic moduli anisotropies, indicating directional instability.

In summary, our findings have significant implications for the design and optimization of UiO-66-based materials. The proposed methodology can be employed to predict the stability of defected UiO-66 structures and guide the selection of optimized defect configurations for specific applications. Moreover, future studies should consider the impact of defect distribution and orientation on amorphization pressure and elastic properties to obtain a more comprehensive understanding of UiO-66-based materials' behavior.

CRediT authorship contribution statement

Esteban Acuna-Yeomans: Writing – review & editing, Writing – review & editing, Visualization, Validation, Methodology, Investigation, Data curation, Conceptualization. **J.J. Gutiérrez-Sevillano:** Writing – review & editing, Supervision, Project administration. **David Dubbeldam:** Writing – review & editing, Supervision, Resources, Conceptualization. **Sofia Calero:** Writing – review & editing, Supervision, Project administration, Conceptualization.

Declaration of competing interest

The authors declare the following financial interests/personal relationships which may be considered as potential competing interests: Juan Jose Gutierrez Sevillano reports financial support was provided by Spain Ministry of Science and Innovation.

Data availability

Data will be made available on request.

Acknowledgements

The present study was funded by the Eindhoven Institute for Renewable Energy Systems (EIRES). J.J.G.S thanks to the Spanish Ministerio de Ciencia e Innovacion for its financial support (CNS2022-136163).

Appendix A. Supplementary data

Supplementary data to this article can be found online at https://doi.org/10.1016/j.micromeso.2023.112922.

References

[1] H. Li, M. Eddaoudi, M. O'Keeffe, O.M. Yaghi, Design and synthesis of an exceptionally stable and highly porous metal-organic framework, Nature (1999), https://doi.org/10.1038/46248.

[2] C. Livage, N. Guillou, J. Marrot, G. Férey, Construction of two- and three-dimensional coordination polymers from cobalt trimesate, Chem. Mater. (2001), https://doi.org/10.1021/cm011115k.

[3] S. Kitagawa, R. Kitaura, S. Noro, Functional porous coordination polymers, Angew. Chem. Int. Ed (2004), https://doi.org/10.1002/anie.200300610.

[4] H.-C. Zhou, J.R. Long, O.M. Yaghi, Introduction to metal–organic frameworks, Chem. Rev. (2012), https://doi.org/10.1021/cr300014x.

[5] H. Furukawa, K.E. Cordova, M. O'Keeffe, O.M. Yaghi, The chemistry and applications of metal-organic frameworks, Science (2013), https://doi.org/10.1126/science.1230444.

[6] H.-C. "Joe" Zhou, S. Kitagawa, Metal–organic frameworks (MOFs), Chem. Soc. Rev. (2014).

[7] F. Vermoortele, B. Bueken, G. Le Bars, B. Van de Voorde, M. Vandichel, K. Houthoofd, A. Vimont, M. Daturi, M. Waroquier, V. Van Speybroeck, C. Kirschhock, D.E. De Vos, Synthesis modulation as a tool to increase the catalytic activity of metal–organic frameworks: the unique case of UiO-66(Zr), J. Am. Chem. Soc. (2013), https://doi.org/10.1021/ja405078u.

[8] J. Gascon, M.D. Hernández-Alonso, A.R. Almeida, G.P.M. van Klink, F. Kapteijn, G. Mul, Isoreticular MOFs as efficient photocatalysts with tunable band gap: an operando FTIR study of the photoinduced oxidation of propylene, ChemSusChem (2008), https://doi.org/10.1002/cssc.200800203.

[9] A.H. Valekar, K.-H. Cho, S.K. Chitale, D.-Y. Hong, G.-Y. Cha, U.-H. Lee, D. W. Hwang, C. Serre, J.-S. Chang, Y.K. Hwang, Catalytic transfer hydrogenation of ethyl levulinate to γ-valerolactone over zirconium-based metal–organic frameworks, Green Chem. (2016), https://doi.org/10.1039/c6gc00524a.

[10] V.L. Rechac, F.G. Cirujano, A. Corma, F.X. Llabrés i Xamena, Diastereoselective synthesis of pyranoquinolines on zirconium-containing UiO-66 metal-organic frameworks, Eur. J. Inorg. Chem. (2016), https://doi.org/10.1002/ejic.201600372.

[11] P. Horcajada, R. Gref, T. Baati, P.K. Allan, G. Maurin, P. Couvreur, G. Férey, R. E. Morris, C. Serre, Metal–organic frameworks in biomedicine, Chem. Rev. (2011), https://doi.org/10.1021/cr200256v.

[12] C.A. Trickett, A. Helal, B.A. Al-Maythalony, Z.H. Yamani, K.E. Cordova, O. M. Yaghi, The chemistry of metal–organic frameworks for CO2 capture, regeneration and conversion, Nat. Rev. Mater. (2017), https://doi.org/10.1038/natrevmats.2017.45.

[13] T.G. Grissom, D.M. Driscoll, D. Troya, N.S. Sapienza, P.M. Usov, A.J. Morris, J. R. Morris, Molecular-level insight into CO2 adsorption on the zirconium-based metal–organic framework, UiO-66: a combined spectroscopic and computational approach, J. Phys. Chem. C (2019), https://doi.org/10.1021/acs.jpcc.9b02513.

[14] C. Petit, Present and future of MOF research in the field of adsorption and molecular separation, Current Opinion in Chemical Engineering (2018), https://doi.org/10.1016/j.coche.2018.04.004.

[15] J.-R. Li, R.J. Kuppler, H.-C. Zhou, Selective gas adsorption and separation in metal–organic frameworks, Chem. Soc. Rev. (2009), https://doi.org/10.1039/b802426j.

[16] J.H. Cavka, S. Jakobsen, U. Olsbye, N. Guillou, C. Lamberti, S. Bordiga, K. P. Lillerud, A new zirconium inorganic building brick forming metal organic frameworks with exceptional stability, J. Am. Chem. Soc. (2008), https://doi.org/10.1021/ja8057953.

[17] L. Valenzano, B. Civalleri, S. Chavan, S. Bordiga, M.H. Nilsen, S. Jakobsen, K. P. Lillerud, C. Lamberti, Disclosing the complex structure of UiO-66 metal organic framework: a synergic combination of experiment and theory, Chem. Mater. (2011), https://doi.org/10.1021/cm1022882.

[18] J.B. DeCoste, G.W. Peterson, H. Jasuja, T.G. Glover, Y. Huang, K.S. Walton, Stability and degradation mechanisms of metal–organic frameworks containing the Zr6O4(OH)4 secondary building unit, J. Mater. Chem. A (2013), https://doi.org/10.1039/c3ta10662d.

[19] K. Leus, T. Bogaerts, J. De Decker, H. Depauw, K. Hendrickx, H. Vrielinck, V. Van Speybroeck, P. Van Der Voort, Systematic study of the chemical and hydrothermal stability of selected "stable" Metal Organic Frameworks, Microporous Mesoporous Mater. (2016), https://doi.org/10.1016/j.micromeso.2015.11.055.

[20] PascalG. Yot, K. Yang, F. Ragon, V. Dmitriev, T. Devic, P. Horcajada, C. Serre, G. Maurin, Exploration of the mechanical behavior of metal organic frameworks UiO-66(Zr) and MIL-125(Ti) and their NH2functionalized versions, Dalton Trans. (2016), https://doi.org/10.1039/c5dt03621f.

[21] H. Wu, T. Yildirim, W. Zhou, Exceptional mechanical stability of highly porous zirconium metal–organic framework UiO-66 and its important implications, J. Phys. Chem. Lett. (2013), https://doi.org/10.1021/jz4002345.

[22] G.C. Shearer, S. Chavan, S. Bordiga, S. Svelle, U. Olsbye, K.P. Lillerud, Defect engineering: tuning the porosity and composition of the metal–organic framework UiO-66 via modulated synthesis, Chem. Mater. (2016), https://doi.org/10.1021/acs.chemmater.6b00602.

[23] L. Liu, Z. Chen, J. Wang, D. Zhang, Y. Zhu, S. Ling, K.-W. Huang, Y. Belmabkhout, K. Adil, Y. Zhang, B. Slater, M. Eddaoudi, Y. Han, Imaging defects and their evolution in a metal–organic framework at sub-unit-cell resolution, Nat. Chem. (2019), https://doi.org/10.1038/s41557-019-0263-4.

[24] G.C. Shearer, S. Chavan, J. Ethiraj, J.G. Vitillo, S. Svelle, U. Olsbye, C. Lamberti, S. Bordiga, K.P. Lillerud, Tuned to perfection: ironing out the defects in metal–organic framework UiO-66, Chem. Mater. (2014), https://doi.org/10.1021/cm501859p.

[25] M.J. Cliffe, W. Wan, X. Zou, P.A. Chater, A.K. Kleppe, M.G. Tucker, H. Wilhelm, N. P. Funnell, F.-X. Coudert, A.L. Goodwin, Correlated defect nanoregions in a metal–organic framework, Nat. Commun. (2014), https://doi.org/10.1038/ncomms5176.

[26] H. Wu, Y.S. Chua, V. Krungleviciute, M. Tyagi, P. Chen, T. Yildirim, W. Zhou, Unusual and highly tunable missing-linker defects in zirconium metal–organic framework UiO-66 and their important effects on gas adsorption, J. Am. Chem. Soc. (2013), https://doi.org/10.1021/ja404514r.

[27] P. Ghosh, Y.J. Colón, R.Q. Snurr, Water adsorption in UiO-66: the importance of defects, Chem. Commun (2014), https://doi.org/10.1039/c4cc04945d.

[28] A.W. Thornton, R. Babarao, A. Jain, F. Trousselet, F.-X. Coudert, Defects in metal–organic frameworks: a compromise between adsorption and stability? Dalton Trans. (2016) https://doi.org/10.1039/c5dt04330a.

[29] W. Liang, C.J. Coghlan, F. Ragon, M. Rubio-Martinez, D.M. D'Alessandro, R. Babarao, Defect engineering of UiO-66 for CO2 and H2O uptake – a combined experimental and simulation study, Dalton Trans. (2016), https://doi.org/10.1039/c6dt00189k.

[30] J. Canivet, M. Vandichel, D. Farrusseng, Origin of highly active metal–organic framework catalysts: defects? Defects! Dalton Trans. (2016) https://doi.org/10.1039/c5dt03522h.

[31] J.M. Taylor, S. Dekura, R. Ikeda, H. Kitagawa, Defect control to enhance proton conductivity in a metal–organic framework, Chem. Mater. (2015), https://doi.org/10.1021/acs.chemmater.5b00665.

[32] J.M. Taylor, T. Komatsu, S. Dekura, K. Otsubo, M. Takata, H. Kitagawa, The role of a three dimensionally ordered defect sublattice on the acidity of a sulfonated metal–organic framework, J. Am. Chem. Soc. (2015), https://doi.org/10.1021/jacs.5b07267.

[33] M.J. Cliffe, J.A. Hill, C.A. Murray, F.-X. Coudert, A.L. Goodwin, Defect-dependent colossal negative thermal expansion in UiO-66(Hf) metal–organic framework, Phys. Chem. Chem. Phys. (2015), https://doi.org/10.1039/c5cp01307k.

[34] M.I. Hossain, J.D. Cunningham, T.M. Becker, B.E. Grabicka, K.S. Walton, B. D. Rabideau, T.G. Glover, Impact of MOF defects on the binary adsorption of CO2 and water in UiO-66, Chem. Eng. Sci. (2019), https://doi.org/10.1016/j.ces.2019.03.053.

[35] A. Planchais, S. Devautour-Vinot, F. Salles, F. Ragon, T. Devic, C. Serre, G. Maurin, A joint experimental/computational exploration of the dynamics of confined water/Zr-based MOFs systems, J. Phys. Chem. C (2014), https://doi.org/10.1021/jp5039267.

[36] S. Wang, G. Zhou, Y. Sun, L. Huang, A computational study of water in UiO-66 Zr-MOFs: diffusion, hydrogen bonding network, and confinement effect, AIChE J. (2020), https://doi.org/10.1002/aic.17035.

[37] Q. Yang, V. Guillerm, F. Ragon, A.D. Wiersum, P.L. Llewellyn, C. Zhong, T. Devic, C. Serre, G. Maurin, CH4 storage and CO2 capture in highly porous zirconium oxide based metal–organic frameworks, Chem. Commun. (2012), https://doi.org/10.1039/c2cc34714h.

[38] G. Jajko, J.J. Gutiérrez-Sevillano, A. Sławek, M. Szufla, P. Kozyra, D. Matoga, W. Makowski, S. Calero, Water adsorption in ideal and defective UiO-66 structures, Microporous Mesoporous Mater. (2022), https://doi.org/10.1016/j.micromeso.2021.111555.

[39] P.G. Boyd, S.M. Moosavi, M. Witman, B. Smit, Force-field prediction of materials properties in metal-organic frameworks, J. Phys. Chem. Lett. (2017), https://doi.org/10.1021/acs.jpclett.6b02532.

[40] A.K. Rappe, C.J. Casewit, K.S. Colwell, W.A. Goddard III, W.M. Skiff, UFF, a full periodic table force field for molecular mechanics and molecular dynamics simulations, J. Am. Chem. Soc. (1992), https://doi.org/10.1021/ja00051a040.

[41] D.E. Coupry, M.A. Addicoat, T. Heine, Extension of the universal force field for metal–organic frameworks, J. Chem. Theory Comput. (2016), https://doi.org/10.1021/acs.jctc.6b00664.

[42] J.K. Bristow, D. Tiana, A. Walsh, Transferable force field for metal–organic frameworks from first-principles: BTW-FF, J. Chem. Theor. Comput. (2014), https://doi.org/10.1021/ct500515h.

[43] S.M.J. Rogge, J. Wieme, L. Vanduyfhuys, S. Vandenbrande, G. Maurin, T. Verstraelen, M. Waroquier, V. Van Speybroeck, Thermodynamic insight in the high-pressure behavior of UiO-66: effect of linker defects and linker expansion, Chem. Mater. (2016), https://doi.org/10.1021/acs.chemmater.6b01956.

[44] L. Vanduyfhuys, S. Vandenbrande, T. Verstraelen, R. Schmid, M. Waroquier, V. Van Speybroeck, QuickFF: a program for a quick and easy derivation of force fields for metal-organic frameworks from ab-initio input, J. Comput. Chem. (2015), https://doi.org/10.1002/jcc.23877.

[45] A.U. Ortiz, A. Boutin, A.H. Fuchs, F.-X. Coudert, Anisotropic elastic properties of flexible metal-organic frameworks: how soft are soft porous crystals? Phys. Rev. Lett. (2012) https://doi.org/10.1103/physrevlett.109.195502.

[46] A. Marmier, Z.A.D. Lethbridge, R.I. Walton, C.W. Smith, S.C. Parker, K.E. Evans, ElAM: a computer program for the analysis and representation of anisotropic elastic properties, Comput. Phys. Commun. (2010), https://doi.org/10.1016/j.cpc.2010.08.033.

[47] S.M.J. Rogge, M. Waroquier, V. Van Speybroeck, Reliably modeling the mechanical stability of rigid and flexible metal–organic frameworks, Acc. Chem. Res. (2017), https://doi.org/10.1021/acs.accounts.7b00404.
[48] J.F. Lutsko, Stress and elastic constants in anisotropic solids: molecular dynamics techniques, J. Appl. Phys. (1988), https://doi.org/10.1063/1.341877.
[49] K. Van Workum, G. Gao, J.D. Schall, J.A. Harrison, Expressions for the stress and elasticity tensors for angle-dependent potentials, J. Chem. Phys. (2006), https://doi.org/10.1063/1.2338522.
[50] G. Clavier, A.P. Thompson, Computation of the thermal elastic constants for arbitrary manybody potentials in LAMMPS using the stress-fluctuation formalism, Comput. Phys. Commun. (2023), https://doi.org/10.1016/j.cpc.2023.108674.
[51] A.P. Thompson, H.M. Aktulga, R. Berger, D.S. Bolintineanu, W.M. Brown, P. S. Crozier, P.J. in 't Veld, A. Kohlmeyer, S.G. Moore, T.D. Nguyen, R. Shan, M. J. Stevens, J. Tranchida, C. Trott, S.J. Plimpton, Lammps - a flexible simulation tool for particle-based materials modeling at the atomic, meso, and continuum scales, Comput. Phys. Commun. (2022), https://doi.org/10.1016/j.cpc.2021.108171.
[52] S.M.J. Rogge, L. Vanduyfhuys, A. Ghysels, M. Waroquier, T. Verstraelen, G. Maurin, V. Van Speybroeck, A comparison of barostats for the mechanical characterization of metal–organic frameworks, J. Chem. Theory Comput. (2015), https://doi.org/10.1021/acs.jctc.5b00748.
[53] R. Gaillac, P. Pullumbi, F.-X. Coudert, ELATE: an open-source online application for analysis and visualization of elastic tensors, J. Phys. Condens. Matter (2016), https://doi.org/10.1088/0953-8984/28/27/275201.
[54] H. Wu, T. Yildirim, W. Zhou, Exceptional mechanical stability of highly porous zirconium metal–organic framework UiO-66 and its important implications, J. Phys. Chem. Lett. (2013), https://doi.org/10.1021/jz4002345.